STATISTICAL AND 3D NONLINEAR FINITE ELEMENT ANALYSIS OF SCHLEGEIS DAM

VICTOR SAOUMA, ERIC HANSEN, BALAJI RAJAGOPALAN

DEPT. OF CIVIL ENGINEERING, UNIVERSITY OF COLORADO, BOULDER

ABSTRACT: This submission is composed of two parts. First a statistical analysis of the dam crest displacement is performed, along with a prediction for the years 2000-2001. Then a 3D finite element analysis of Schlegeis dam is performed using an internally generated finite element mesh (based on the mathematical description of the geometry). Finally, both analysis results are examined in light of the ICOLD Theme-C organizers questions.

1 Introduction

This paper is the formal submission to the problem posed by the organizers of Theme-C of the Sixth Benchmark Workshop on Numerical Analysis of Dams, (Verbundplan 2001).

It is composed of two parts. First a detailled statistical analysis, and prediction for pendulum displacement is performed. Both a stepwise linear regression and a K-Nearest neighbor local polynomial technique are used. Then, a 3D finite element analysis of the dam with only hydrostatic load (due to lack of time, the thermal analysis was not performed) is performed. Rather than using the finite element mesh provided by the organizers, it was decided to begin with the mathematical description of the arch dam. Using Mathematica (Wolfram 1999) for symbolic operations, elliptical arches were then defined, using our in-house mesh generator KumoNoSu (Hansen and Saouma 2001) a 3D mesh of 4 noded tetrahedron elements was generated, and finally analysis was performed with our finite element code Merlin (Reich, Červenka and Saouma 1997), and visualized with our graphical post-processor Spider (Haussman and Saouma 1998). KumoNoSu is based on the T3D program of Rypl (1998).

It should be clearly stated that our contribution was primarily driven by an intellectual curiosity in testing innovative statistical techniques, and in assessing the performance of our in-house specialized software.

1.1 Problem Description

Schlegeis arch dam was constructed between 1969 and 1971. It is a double curvature arch/gravity dam with a crest length/dam height ratio of 5.5. The foundation of the dam consists of fairly uniform granitic mica gneiss. Its plane of schistosity strikes approximately parallel to the right bank abutment and has a very steep dip towards downstream. The dam consists of 43 blocks, each 17 m wide. It is provided with 4 horizontal inspection galleries and the base gallery located at the foundation rock. It has a crest elevation of 1,783 m, height of 131 m, crest length of 725 m, crest thickness of 9 m, and base thickness of 34 m. Water level is between 1,680 and 1,782 m.

1.2 Field Measurements

Field measurements, as reported by the workshop organizers, include water elevation, plum line displacement, concrete temperature at three locations (close to upstream face, center, close to downstream face) at two different elevations (12 and ss m), and air temperature, Fig. 1.

2 Statistical Analysis

Statistical functional estimation techniques were used to predict the pendulum using a subset of predictors. First, the correlation matrix containing the correlations among the predictors and to pendulum was determined, Table 1. It was noted that the pendulum has a strong positive correlation with WL (Water Level), H_{12}^{mi} and H_{15}^{up}. It has a significant negative correlation with T_{air} and H_{12}^{up}.

	Pend.	WL	T_{air}	H_12^{up}	H_{12}^{mi}	H_{12}^{dw}	H_{15}^{up}	H_{15}^{m}i	H_{15}^{dw}
Pend	1.0000	0.7751	-0.3319	-0.3168	0.7607	-0.2027	0.4261	0.3377	-0.1355
WL	0.7751	1.0000	0.1147	0.2114	0.7300	0.3649	0.7578	-0.0761	0.4374
T_{air}	-0.3319	0.1147	1.0000	0.6933	-0.2683	0.7672	0.2369	-0.6445	0.7365
H_{12}^{up}	-0.3168	0.2114	0.6933	1.0000	-0.1761	0.8790	0.4388	-0.7436	0.8597
H_{12}^{mi}	0.7607	0.7300	-0.2683	-0.1761	1.0000	-0.0655	0.6929	0.3406	0.0231
H_{12}^{dw}	-0.2027	0.3649	0.7672	0.8790	-0.0655	1.0000	0.5526	-0.7070	0.9905
H_{15}^{up}	0.4261	0.7578	0.2369	0.4388	0.6929	0.5526	1.0000	-0.1161	0.6300
H_{15}^{mi}	0.3377	-0.0761	-0.6445	-0.7436	0.3406	-0.7070	-0.1161	1.0000	-0.6672
H_{15}^{dw}	-0.1355	0.4374	0.7365	0.8597	0.0231	0.9905	0.6300	-0.6672	1.0000

Table 1: Correlation Coefficients

Then, two statistical techniques (i) Stepwise Linear Regression and (ii) K-nearest neighbor Local Polynomial technique were used in the investigation.

In order to assess the quality of the two models, the data up to May 1996 was used to perform a preliminary prediction for the period June 1996 - June 1997 (1,600 points). This exercise was to compare the two methods in a prediction mode. Then the models were fit on data prior to Dec. 1998 (400 points). Finally prediction of the pendulum for the period Jan 1999 - Jan 2001 was made based on all 2,557 data points with pendulum reading.

The two methods are briefly described followed by a discussion of the results.

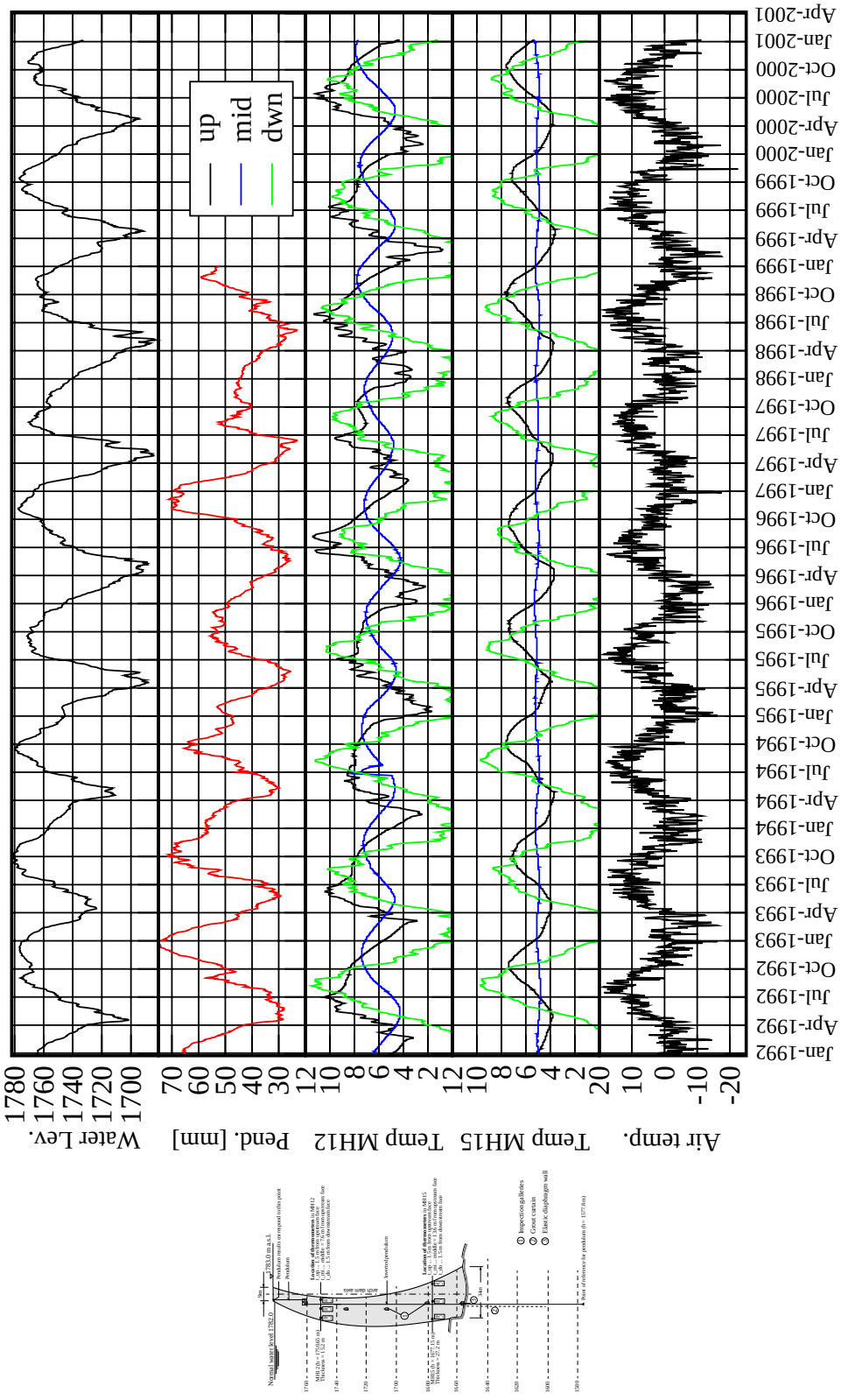

Figure 1: Recorded Field Data, (Verbundplan 2001)

2.1 Statistical Methods

2.1.1 Stepwise Linear Regression

This technique is an extension of the widely used linear regression. The theory of linear regression is established strongly and requires no discussion. The Stepwise linear regression method identifies the best subset of predictors (from the predictors shown in table 1) that gives the highest adjusted R-square. Other criteria, instead of R-square can also be chosen, e.g., Mallow's Cp statistic. Generally, the results turn out to be very similar regardless of the statistic. The method performs a linear regression with all combinations of predictors and selects the best subset of predictors based on the chosen statistic. In this case the method suggested a best subset of predictors consisting of WL, T_{air}, H_{12}^{up}, H_{12}^{dw}, H_{12}^{dw}, H_{15}^{up}, H_{15}^{mi}, and H_{15}^{dw}. Details of this method can be found in (Radhakrishna Rao and Toutenburg 1995) and (Weisberg 1985).

2.1.2 K-Nearest Neighbor Local Polynomial Technique

Linear regression is easily implemented and works very well when the relationship is truly linear. If there are nonlinearities present then this method is inadequate, and one has to resort to higher order polynomials. Nonparametric techniques provide a flexible alternative. There are various nonparametric schemes, but we use the K-nearest neighbor local polynomial technique, for its ease in implementation and understanding. Essentially the method involves selecting K-nearest neighbors to a predictor point and fitting a polynomial to this. The fitted polynomial is then used for estimation. Two predictors were picked for this method WL and H_{12}^{up} unlike a larger set of predictors in the linear regression. Those predictors were selected by trial and error, however one can use objective criteria described in the following section for predictor selection. The details of this method can be obtained from (Rajagopalan and Lall 1998). Below we provide a brief description of the method abstracted from this paper for the benefit of the reader.

Local polynomial estimators for function estimation are one of the many non-parametric estimators that are in practice. Nonparametric or local fitting estimators, with weaker assumptions than the parametric estimators (e.g. kriging), adapt better to heterogeneous and non-stationary data sets. Some attributes of these estimators are:

1. The estimator can often be expressed as a weighted moving average of the observations.

2. The estimates are defined locally or using data from a small neighborhood of each point of estimate. Consequently, they can approximate a wide class of target, underlying functions.

3. The nonparametric estimator has parameters that control the local weights and the size of the neighborhood used for estimation.

2.1.2.1 Local Polynomial Scheme Consider a general regression model given as:

$$\mathbf{y} = \mathbf{f}(\mathbf{x}) + \mathbf{e}, \quad i = 1, \cdots, n \tag{1}$$

$$\mathbf{y}_i = \mathbf{f}(\mathbf{x}_i) + \mathbf{e}_i, \quad i = 1, \cdots, n \tag{2}$$

where $\mathbf{x}$ is a vector of M explanatory variables, $\mathbf{y}$ is the "response" variable, $\mathbf{f}(.)$ represents the underlying functional relationship between $\mathbf{y}$ and $\mathbf{x}$, $\mathbf{e}_i$ are noise or measurement errors, that may or may not depend on $\mathbf{x}_i$, and n is the number of observations.

Generally, the strategy is to choose a certain number, k, of nearest neighbors (in terms of Euclidean distance) of the estimation point x, and to form the estimate $f(x)$ through a locally weighted, polynomial regression over the $(\mathbf{x}, \mathbf{y})$ data that lie in the neighborhood. The sampling locations $\mathbf{x}_i$ are usually not regularly spaced. We assume the e_i are uncorrelated, mean zero, random variables, assumed to be approximately identically distributed in the k nearest neighborhood of the point of estimate. Then, the locally weighted polynomial regression at each point of estimate $x_l^*, l = 1, ?, np$, given a (n by M) data matrix x and a (n by 1) response vector y, is obtained through the solution of the weighted least squares problem:

$$\text{Min}(\mathbf{y}_l - \mathbf{Z}_l\mathbf{b}_l)^T\mathbf{W}_l(\mathbf{y}_l - \mathbf{Z}_l\mathbf{b}_l) \tag{3}$$

where the subscript l recognizes that the associated element is connected with the point of estimate $\mathbf{x}_l^*$; $\mathbf{b}_l$ are estimates of the coefficients of the terms in the basis defined by $\mathbf{Z}_l$; $\mathbf{Z}_l$ is a matrix formed by augmenting $\mathbf{x}$, with columns that represent the polynomial expansion of $\mathbf{x}$ to degree p (including cross product terms if desired); W_l is a k by k diagonal weight matrix with elements

$$w_{ii,l} = \frac{K(u_{i,l})}{\sum_{j=1}^{k}(u_{j,l})} \tag{4}$$

where $u_{i,l} = d_{i,l}/d_{k,l}$; $d_{i,l}$ is the distance from x_l^* to x_i using an appropriate metric, and $K(.)$ is a weight function. We have implemented a bisquare kernel ($K(u) = 15/16(1-u^2)^2$). The matrix Z_l and vector y_l are defined over the k nearest neighborhood of x_l^*. Singular Value Decomposition (SVD) is used to solve the linear estimation problem resulting from Eq. 3. The coefficients b_l are obtained as:

$$\mathbf{b}_l = (\mathbf{Z}_l\mathbf{W}_l\mathbf{Z}_l)^{-1}\mathbf{W}_l\mathbf{y}_l \tag{5}$$

The resulting estimate of $\hat{f}(x_l^*)$ is then

$$\hat{f}(x_l^*) = \mathbf{z}_l\mathbf{b}_l \tag{6}$$

where $\mathbf{z}_l$ is the d by l vector formed by augmenting $\mathbf{x}_l$ with polynomial terms of order p, and retaining the terms for which $\mathbf{b}_j$ are found to be significantly different from 0.

2.1.2.2 Parameter selection k & p The Generalized Cross Validation (GCV) statistic is given by

$$\mathrm{GCV}(\hat{f}) = \frac{\mathrm{MSE}(\hat{f})}{(n^{-1}\mathrm{tr}\ [\mathbf{I} - \mathbf{H}])^2} \tag{7}$$

where the Mean Square Error MSE is given by

$$(\hat{f}) = n^{-1}\sum_{i=1}^{n}(y_i - \hat{f}(\mathbf{x}_i))^2 \tag{8}$$

$\mathbf{H}$ is the influence matrix defined through

$$\hat{f} = \mathbf{H}\mathbf{y} \tag{9}$$

Note that this equation represents a linear estimator, and the i^{th} diagonal element of $\mathbf{H}$ can be thought of as the "weight" of that data point on the estimate at that point.

We shall consider the whole data set for parameter selection. The global GCV (GGCV) can be estimated after performing n local regressions at each data point $\mathbf{x}_i$ $(i = 1, \cdots, n)$, as:

$$\mathrm{GGCV}(\hat{f}) = \frac{\frac{\sum_{i=1}^{n} e_i^2}{n}}{\left(1 - \sum_{i=1}^{n} \frac{h_{ii}}{n}\right)^2} \tag{10}$$

where h_{ii} is estimated from equation Eq. 9, and where $e_i = y_i - \hat{f}(\mathbf{x}_i)$

One can select appropriate values of k and p, as the minimizers of the GGCV value computed in Eq. 10 for each combination of k and p. These would be the values of k and p that would do well on the average. However, in certain situations (e.g., where the curvature of the target function varies over the data, and where the variance of the noise varies over the range of the data), one may wish to make such choices locally at the point of estimate. Accordingly, the local GCV (LGCV) score is then given as:

$$\mathrm{LGCV}_l(\hat{f}) = \frac{e_l^T \mathbf{W}_l e_l}{\left(\frac{k-d}{x}\right)^2} \tag{11}$$

The appropriate values of k and p can then be obtained as the ones that minimize the local GCV score for the local regression. The LGCV_l value also provides insight into the local predictive error variance.

For this data a K (the number of neighbors) of 80 and a local linear polynomial was found to be optimal. This is used in the forecasts.

2.2 Result Interpretation

Figure 2 shows the actual Pendulum values and predicted values from the linear regression technique and the K-nearest neighbor local polynomial technique. It can be seen that the nonparametric technique predicts the values much better than the linear regression. In particular, the peak is underestimated in the linear regression, which is consistent with linear regression. The nonparametric technique predicts the pendulum values very well and also it is highly parsimonious relative to the linear regression technique.

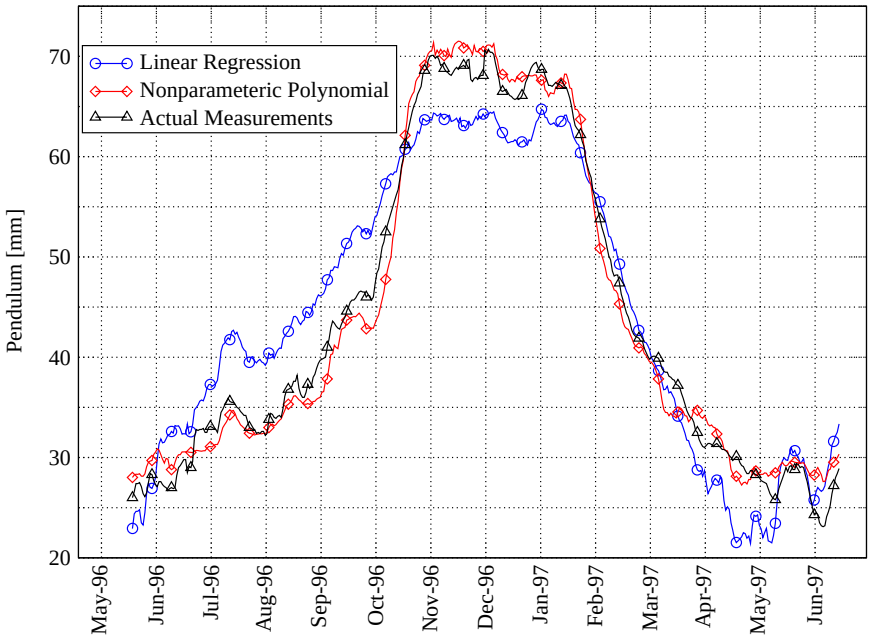

Figure 2: Linear and Nonparameteric Polynomial Validation

The forecast for the period Jan 1999 - Dec 2001 is shown in Figure 3, the peaks are much smoother than in the case of linear regression. We also show forecast from another nonparametric technique called Local Regression (Loader 1999). This is very similar to the K-nearest neighbor local polynomial technique described above, except that its implementation is slightly different. It can be seen that the forecast from the two nonparametric techniques are very close to each other.

3 Finite Element Analysis

3.1 Mathematical Description

Whereas circular arches are favored in the design of US arch dams, (Anonym. 1977), European ones are based on conic surfaces[1]. Schlegeis dam, is no exception.

Hence, we decided to test the capabilities of our recently developed mesh generator KumoNoSu in generating 3D data of an arch dam which can be mathematically defined.

The dam geometry is best described through Fig. 4, where the quadratic equation of an arch is given by

$$x^2 + (1 - \varepsilon^2)(y - y_s)^2 - 2\rho_s(y - y_s) = 0 \tag{12}$$

where x and y are the coordinates of the arch center line, y_s the coordinate of the center cantilever, ε corresponds to either ε_e (east) or ε_w (west), ρ_s also corresponds to either ρ_e (east) or ρ_w (west). Whereas in the original blue-print, Fig. 4 equations for these control parameters (in terms of the elevation z) were provided, indications are that those do not match the corresponding actual values. Hence, using actual

[1]Probably because of the greater mathematical insight of European Engineers!

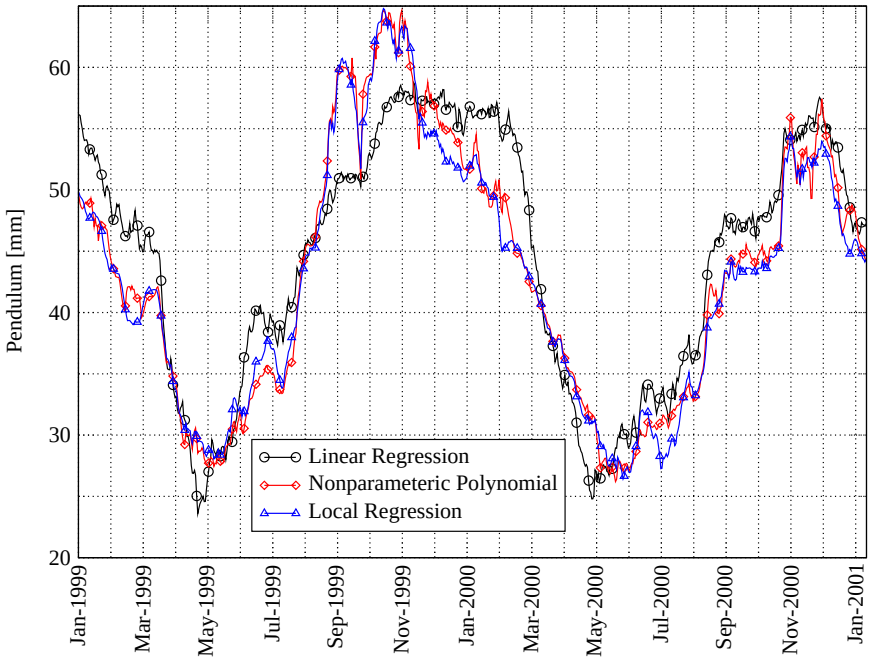

Figure 3: Linear and Nonparameteric Polynomial Future Forecast

data, the following equations were determined through a regression analysis, and provided to us by the organizers:

$$y_s = 0.474883\,(309.903 + 0.559746\,z + 1.9744\,\sqrt{18395.5 + 208.412\,z - 1.\,z^2}) \quad (13)$$

$$\rho_s = 0.456092\,(591.871 - 2.36057\,z - 1.08959\,\sqrt{9111.7 - 172.086\,z + 1.\,z^2}) \quad (14)$$

$$\varepsilon_e^2 = 0.5\,(1.73296 - 0.0132876\,z + 0.00782506\,\sqrt{2978.18 - 102.345\,z + 1.\,z^2}) \quad (15)$$

$$\varepsilon_w^2 = 0.5\,(2.5606 - 0.0119123\,z - 0.0114553\,\sqrt{10264.9 - 200.849\,z + 1.\,z^2}) \quad (16)$$

Substituting, into Eq. 12, we obtain an analytical expression for the y coordinate in terms of x and the elevation z at the arch center line.

Furthermore, the arches have a variable thickness. From the center to x_d (on both the east and the west sides), the arch has a constant thickness x_d, and from x_d to x_k, the arch has a varying thickness given by

$$d = d_s + \frac{(x - x_d)^2}{(x_k - x_d)^2}(d_k - d_s) \quad (17)$$

where x_d, x_k, d_k and d_s are given in Table 2.

3.2 Discretization

3.2.1 Arch

In our investigation, 10 arch elevations were retained (0, 9, 18, 32, 41.519, 50, 70, 90, 110, and 120 m). To each elevation, the corresponding set of parameters were interpolated from Table 2.

KumoNoSu, the 3D mesh generator being used, enables the definition of rational Bezier splines, hence the arches can be correctly represented by a quadratic

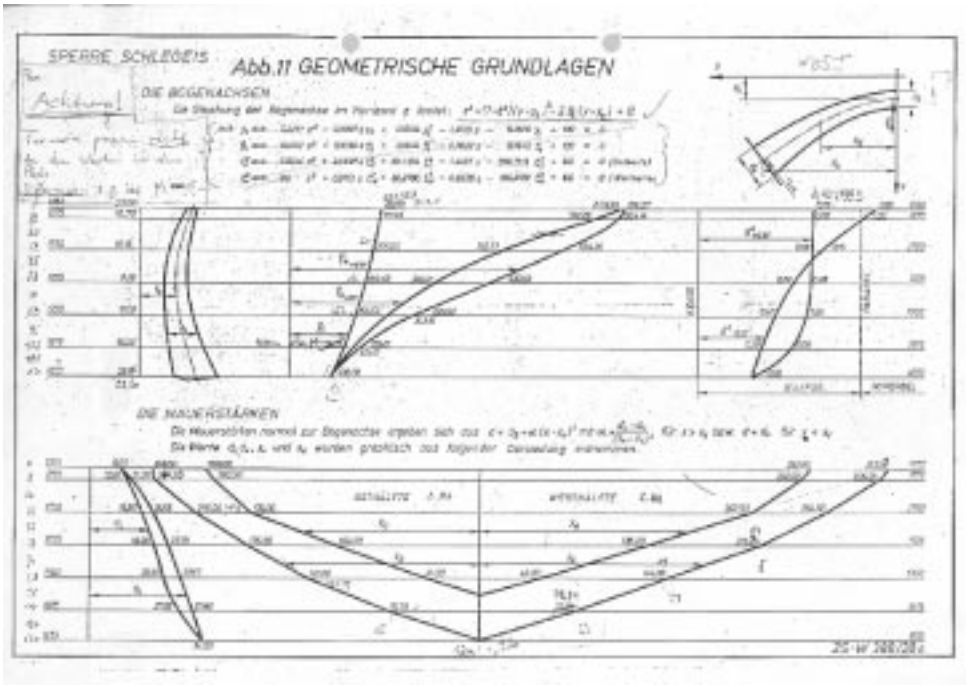

Figure 4: Dam Layout

Var.	Elevations						
	0.	8.	33.	58.	83.	108.	130
West							
x_d	252.	245.16	207.50	128.	49.	11.14	0.
x_k	312.50	301.76	264.50	213.25	144.	73.95	0.
d_s	9.	10.61	15.50	18.98	22.10	27.05	34.0
d_k	9.	12.2	19.55	23.75	27.67	31.60	34.0
East							
x_d	208.	203.	174.	109.	41.	,8.67	0.
x_k	249.5	242.56	216.	176.6	131.	70.75	0.
d_s	9.	10.61	15.50	18.98	22.10	27.05	34.0
d_k	9.	12.2	19.55	23.75	27.67	31.60	34.0

Table 2: Measured Values of Key Variables at Selected Elevations

representation of the spline. The rational Bezier curve has the form

$$\mathbf{P}(t) = \frac{\sum_{i=0}^{n} \omega_i \mathbf{P}_i B_i^n(t)}{\sum_{i=0}^{n} \omega_i B_i^n(t)} \tag{18}$$

where $\mathbf{P}(t)$ is the point on the curve, $\mathbf{P}_i$ are Bezier control points, ω_i are weights of Bezier control points, $B_i^n(t)$ is the Bernstein polynomial

$$B_i^n(t) = \begin{pmatrix} n \\ i \end{pmatrix} t^i (1-t)^{n-i} \tag{19}$$

where t denotes an independent variable varying in the range from 0 to 1, and n is the curve degree. The curve order is equal to $n+1$, $\mathbf{P}_0$ and $\mathbf{P}_n$ correspond to model vertices while the remaining points form the control polygon of the curve. The first and last segments of the control polygon coincide with the curve tangent in the starting and ending vertices respectively.

Interestingly, and perhaps not so coincidentally, Equation 18 is very similar in form with Eq. 5.

For a quadratic representation of an elliptical arc, Fig. 5. we have

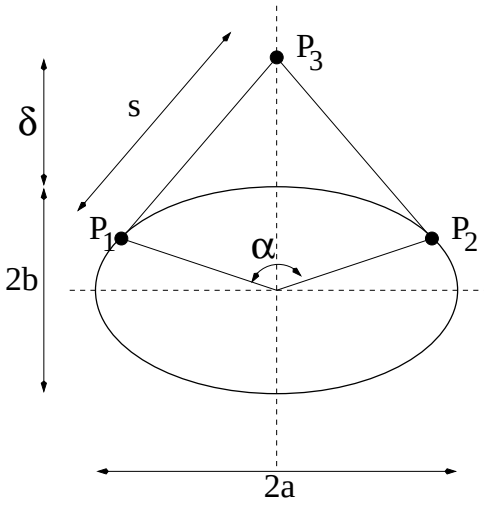

Figure 5: Bezier Polygon for an Elliptical Arc

$$\begin{aligned}
\delta &= b\frac{\sin^2\frac{\alpha}{2}}{\cos\frac{\alpha}{2}} && (20)\\
s &= \frac{\sin\frac{\alpha}{2}}{\cos\frac{\alpha}{2}}\sqrt{a^2\cos^2\frac{\alpha}{2} + b^2\sin^2\frac{\alpha}{2}} && (21)\\
\omega_1 &= \omega_3 = 1 && (22)\\
\omega_3 &= \cos\frac{\alpha}{2} && (23)
\end{aligned}$$

Hence, the Mathematica program provided to us, with the mathematical description of the arches, was modified to determine the Bezier parameters for each of the 10 arches at each elevation (East and West, Upstream and downstream, $0 < x > x_d$

and $x_d < x < x_k$). For each arch, the end points are known, only the control point P_3 and its weight ω_3 had to be determined.

In order to determine the coefficients, it was first noted that the equation of an ellipse is

$$\frac{(x-h)^2}{a^2} + \frac{(y-k)^2}{b^2} = 1 \tag{24}$$

which can be rewritten in normalized form as

$$c_1 x^2 + c_2 y^2 + c_3 x^2 y^2 + c_4 x + c_5 y = 1 \tag{25}$$

where c_3 should be equal to zero and

$$\begin{array}{rcl} c_1 & = & b^2/\Delta \\ c_2 & = & a^2/\Delta \\ c_4 & = & -2b^2h/\Delta \\ c_5 & = & -2a^2k/\Delta \\ \Delta & = & a^2b^2 - b^2h^2 - a^2k^2 \end{array} \tag{26}$$

Hence, the following simple algorithm was implemented with Mathematica:

1. Select arch, z elevation and interpolate control parameters.
2. Determine the corresponding end points.
3. Select three additional internal points which break the arch's x projection into four equal segments.
4. Using Eq. 13-16 and 12, solve for the y coordinate. We now have the x, y, z coordinates at the center line at five points.
5. Determine the five coefficients of the quadratic curve in Eq. 25
6. Solve for the elliptical curve parameters (a, b, h and k) from Eq. 26.
7. Determine the slope, and its normal at each of the five points
8. Determine the thickness at each of the five points, and project half of it to the upstream and the other half to the downstream face along the normal to the slope.
9. Determine the coordinates on the upstream (or downstream) face.
10. Repeat steps 5-6 once for the upstream, and once for the downstream face.
11. From h and k, determine the angle α and solve for the weight of the external control point.
12. Determine the coordinates of point P_3 as being the intersection of the two tangents to the curve at P_1 and P_2.

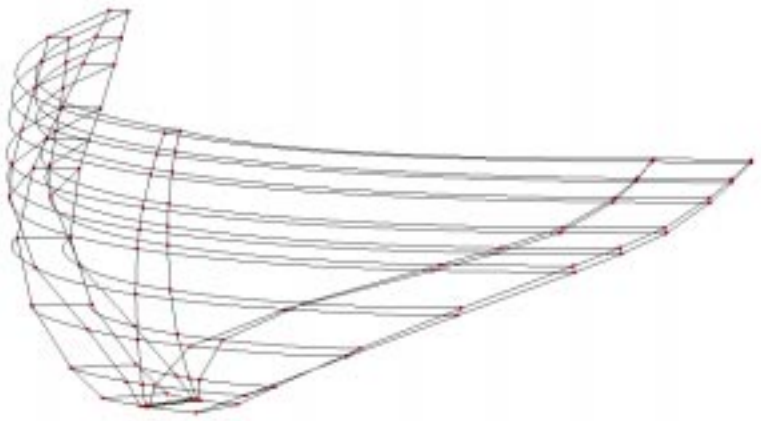

Figure 6: Dam Discretization for Finite Element Mesh Generator

3.2.2 Dam and Foundation

3.2.2.1 Outline Using the procedure previously described, the dam and foundation outlines were subdivided in vertices, curves, and patches as shown in Fig. 6.

3.2.2.2 Finite Element Mesh Finally, the mesh outline shown above was discretized into tetrahedron elements, resulting in the mesh shown in Fig. 7.

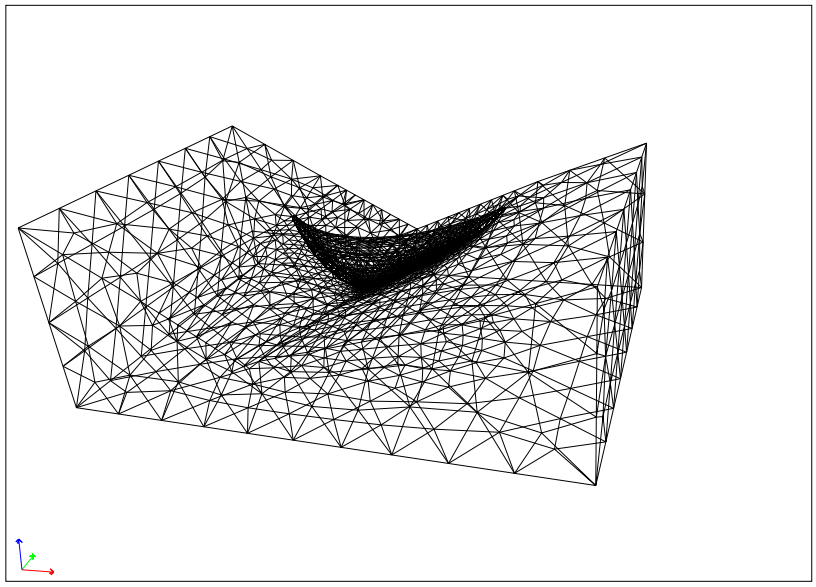

Figure 7: Finite Element Mesh

At this point the reader should be warned not to be misled by the apparent complexity of the resulting mesh. Undoubtedly, when this finite element mesh is compared with the one provided by the organizer of the workshop, it does not look as "nice", however it should be kept in mind that

1. Once the external control point of the dam are known (an essential operation required for any meshing technique), the time needed to triangularize the mesh should be less that the time needed to hand-craft the mesh with brick elements.

2. The element formulation of tetrahedron elements is well established, and there is no reason to suggest that brick elements yield more accurate results than tetrahedron.

3. This meshing technique will result in substantially more nodes/elements than a brick-based finite element mesh.

4. This same mesh can readily be used in conjunction with quadratic, rather than linear finite element mesh, by simply modifying the element type in Merlin.

3.3 Material Properties

The specified material properties are shown in Table 3

		Rock	Concrete
ρ	kg/m^3		2,400
$E_\parallel$	GPA	30	25
$E_\perp$	GPA	10	
ν		0.17	0.17

Table 3: Rock and Concrete Material Properties

Whereas the concrete is homogeneous and isotropic, the rock is reported as being orthotropic and massless. The rock is granite-gneiss with a schistosity of 340/75 degrees related to Gauss-Krüger-System (29.98/75 degrees relative to local Y axis), Fig. 8. An orthotropic material is characterized by 9 independent constants, however

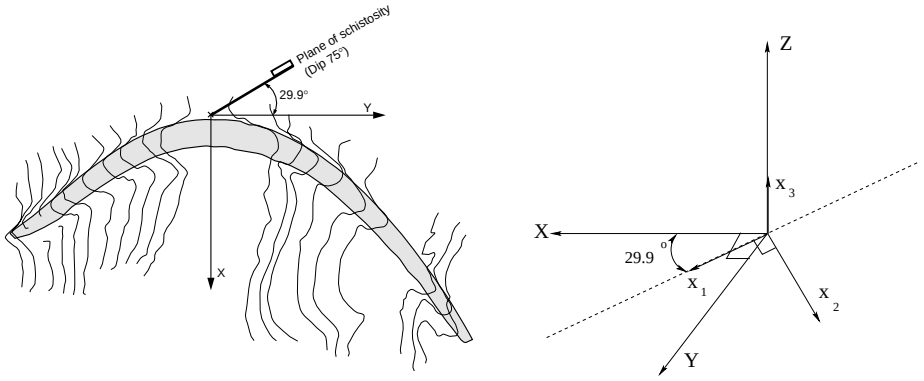

Figure 8: Orthotropic Rock Foundation; Theme-C Coordinate System, and Adopted One

only four were provided. Hence, based on the following assumption, (Lekhnitskii

1981)

$$G_{12} = G_{23} = \frac{E_1 E_2}{E_1(1+2\nu_{12}) + E_2} \tag{27}$$

we select for the orthotropic model of Merlin: E_1=30 GPa; ν_{ij}=0.17, E_2=10 GPa, E_3=10 GPa, $G_{12} = G_{23}$=5.98 GPa, G_{13}=12.82 GPa; $v_x^1 = \cos 29.9 = 0.867$, $v_y^1 = \sin 29.9 = 0.498$, $v_z^1 = 1.0$, $v_x^2 = 0.498$, $v_y^2 = 0.867$, $v_z^2 = 1.0$,

Finally, the interface element properties, (Červenka, Chandra Kishen and Saouma 1998) between the rock and the concrete were assigned the properties shown in Table 4.

f_t'	0.69×10^6	Pa
K_t	2.5×10^{11}	Pa
K_n	2.5×10^{11}	Pa
Φ_F	45^o	
Φ_D	20^o	
G_{I_F}	100	N/m
G_{II_F}	1,000	N/m
γ	0.3	
$u_{D_{max}}$	1×10^{-2}	m
s_1	0.1724×10^6	Pa
w_1	1.08×10^{-4}	m
c_1	0.25×10^6	Pa
cw_1	7.5×10^{-4}	m

Table 4: Interface Element Material Properties

3.4 Analysis

The analysis was performed with the Merlin code. The only source of nonlinearity was the rock concrete interface and the uplift pressure.

Whereas the organizers specified a uniform cracked zone along which the full uplift was to be applied, a different approach was followed in our code.

First the entire rock-concrete contact zone was modeled by interface elements. Then the analysis proceeded incrementally, in terms of pool elevation (the first increment corresponding to the dam self weight which deflection was then subtracted from subsequent analyses). At each pool elevation, a full uplift based on that particular elevation was specified if the interface was to open up. Hence, should the code detect a crack opening, then and only then would the full uplift pressure be applied (Merlin's option to apply a drop in uplift pressure along the uncracked ligament was not activated), Fig. 9.

Finally, it should be noted that each incremental load being specified in terms of its pool elevation, Merlin internally determined both the magnitude of the (triangular) hydrostatic distribution to be applied on all the elements on the upstream face, as well as the magnitude of the full uplift to be applied on the appropriate interface elements, in terms of the spatial coordinates (that is the difference in elevation between Gauss points and pool elevation).

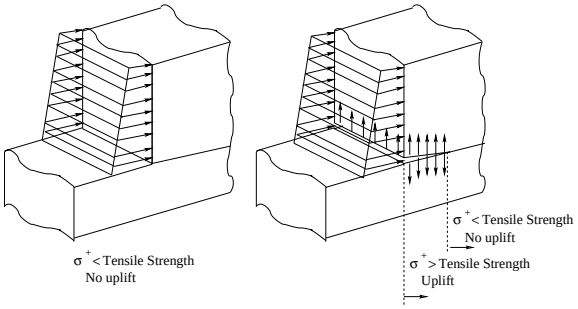

Figure 9: Uplift Modelling

Five analysis were performed:

1. High interface tensile strength 6.894 MPa, no uplift
2. Low interface tensile strength 0.6894 MPA no uplift
3. Low interface tensile strength 0.6894 MPA with uplift
4. Low interface tensile strength 0.6894 MPA no uplift, creep simulated by reducing the concrete's eleastic modulus by a factor of 2.
5. Low interface tensile strength 0.6894 MPA, uplift and "creep"

The final mesh, Fig. 7 consisted in 4,800 nodes, 19,902 linear tetrahedron elements, and 290 interface elements. The input file was 1.8 Mb, the ASCII output file 7.2 Mb, and the `.pst` file for the graphical postprocessor was 347 Mb.

Analyses were performed on a PC, Pentium IV, 1.7 GHz, 264 MB of RAM, took 41 minutes and 15 seconds.

Fig. 10 summarizes the crest displacement relationship in terms of water elevations. Note that the recorded displacement is the radial one of the crest with respect to the (ICOLD) specified reference point.

Fig. 11 illustrates the overall dam/foundation displacements, Fig. 12 shows the interface elements between the dam and the foundation in their deformed shape and contour lines of normal stresses. Note that we are looking into the "lips" of the 3D interface elements opening up and subjected to the uplift pressure. Fig. 13 illustrates the same interface elements, but in their undeformed state, with the normal stresses. Finally, Fig. 14 highlights the dam's deformed shape.

4 Observations, Predictions and Conclusions

Based on the preceding analyses, the following can be drawn:

1. Advanced statistical analysis may indeed provide reasonable predictions to future pendulum displacements, albeit with a lack of physical understanding of the dam response.

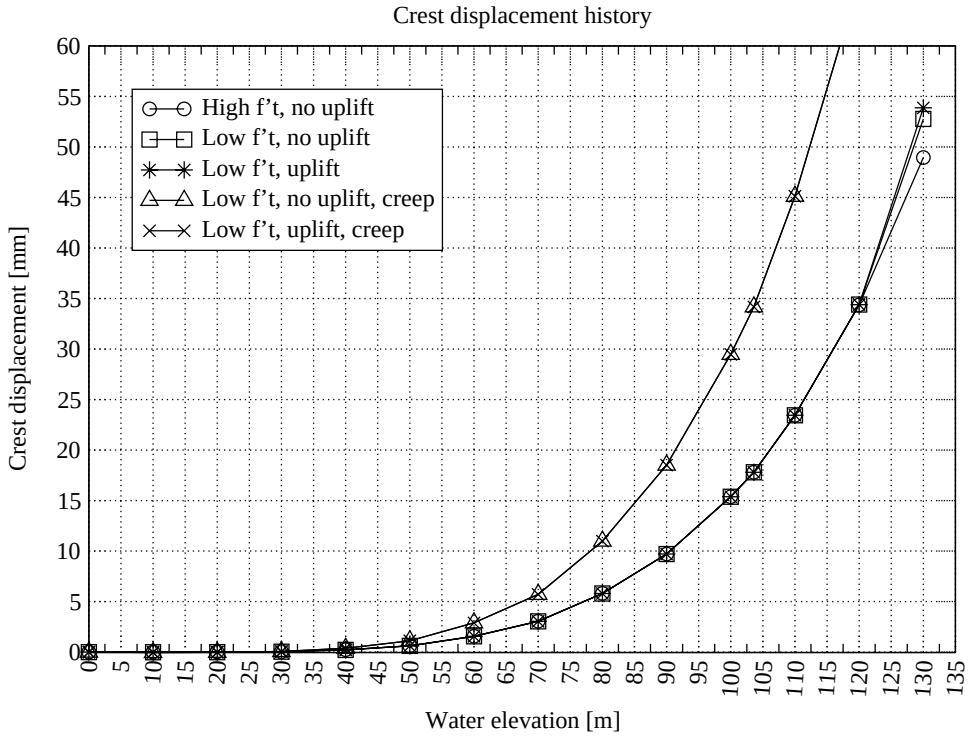

Figure 10: Crest Displacement *vs* Pool Elevation

2. Our prediction for pendulum displacement, based on statistical analysis is shown in Fig. 3. Because of the nature of the technique adopted, it is impossible to determine a closed-form analytical expression.

3. We successfully obtained a finite element mesh based on the analytical description of the dam. Tools such as Mathematica were of great help in such task.

4. We exploited the conical nature of the arches, and the availability of rational Bezier curves in our mesh generator in order to generate the finite element mesh.

5. There is no known reasons for which a tetrahedron based mesh should be inferior to one based on brick elements.

6. Because of time constraint, the finite element analysis restricted itself to variations of the pool elevation.

7. Interface elements were placed between the dam and the foundation.

8. Uplift was correctly measured as taking place only if the foundation has cracked.

9. The effect of uplift is minimal.

10. An incremental analysis was performed to determine the radial crest displacement in terms of pool elevation. Predictions are shown in Fig. 10.

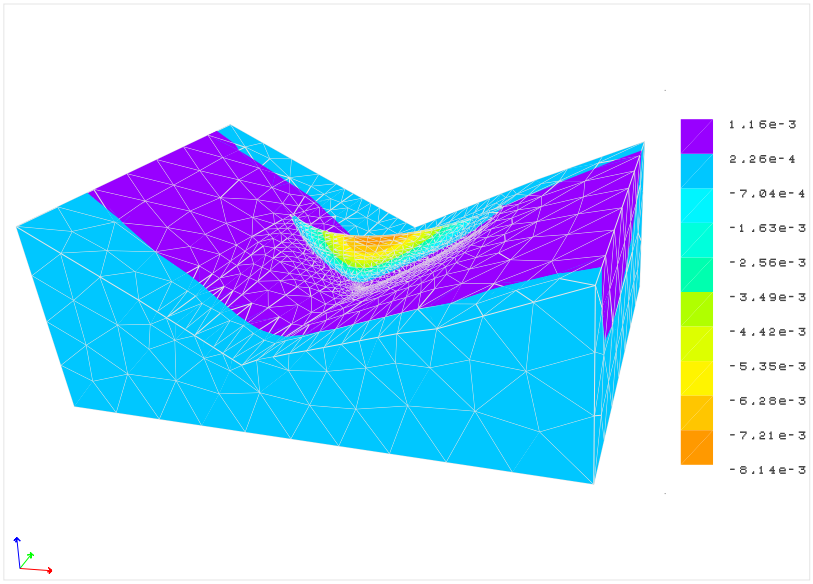

Figure 11: Controur Lines of Radial Displacements

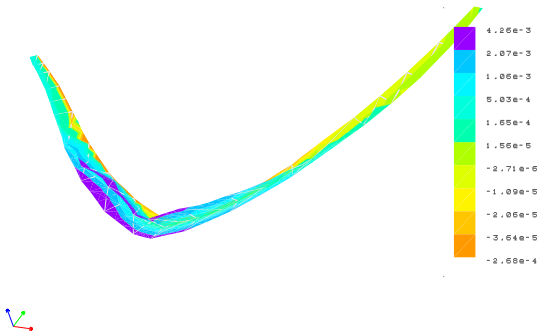

Figure 12: Interface Elements, Deformed Mesh, COD

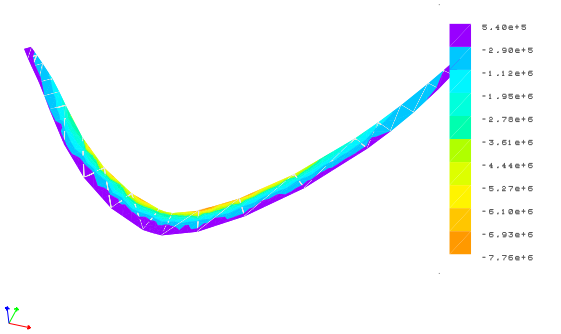

Figure 13: Interface Elements, Normal Stresses

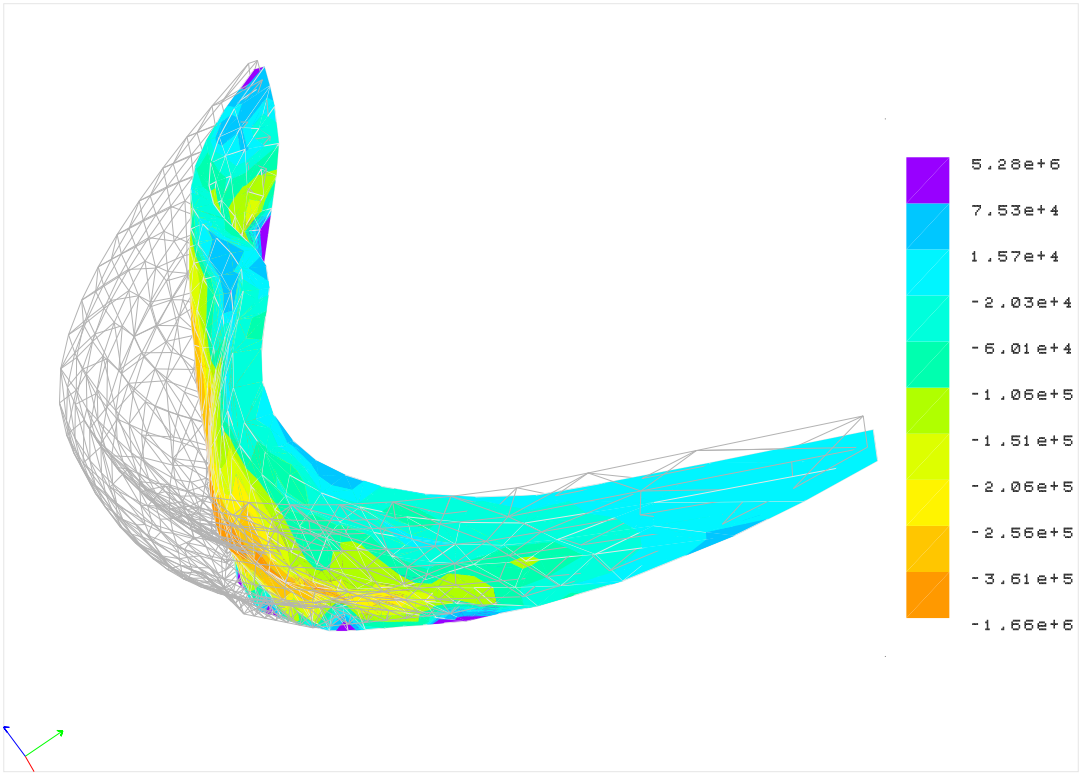

Figure 14: Dam, Deformed Mesh, Contour Lines of Maximum Principal Stresses

11. Creep was addressed by simply reducing the concrete's elastic modulus by 50%. Whereas a creep coefficient of 2.0 is not particularly high, the resulting crest displacements were much higher than the measured ones. Hence, preliminary indications are that creep may not be a major concern for this dam.

12. Because of the nature of the analyses, it is practically impossible to compare predictions based on statistical analysis or on finite element analysis.

13. The recently developed software for mesh generation (KumoNoSu), finite element analysis (Merlin), and graphical post-processor (Spider) appear to have been able to efficiently handle the analysis of arch dams.

5 Acknowledgments

The first author would like to acknowledge the financial support of the Electric Power Research Institute (EPRI, Doug Morris Project Director), and the Tokyo Electric Power Service Company/Tokyo Electric Power Company (TEPSCO/TEPCO, Yoshihisa Uchita Project Director) in the development of both Merlin and KumoNoSu.

References

Anonym.: 1977, Design of arch dams, *Technical report*, U.S.Department of the Interior, Bureau of Reclamation.

Hansen, E. and Saouma, V.: 2001, Kumonosu, a 3d intereactive graphics mesh generator for merlin, *Technical report*, Report Submitted by the University of Colorado to the Tokyo Electric Power Service Company. `http://civil.colorado.edu/~saouma/Kumo`.

Haussman, G. and Saouma, V.: 1998, Spider, a 3d intereactive graphics finite element post-processor, *Technical report*, Report Submitted by the University of Colorado to the Electric Power Research Institute, Palo Alto. `http://civil.colorado.edu/~saouma/Spider`.

Lekhnitskii, S.: 1981, *Theory of Elasticity of an Anisotropic Body*, Mir, Moscow (English Translation).

Loader, c.: 1999, *Local Regression and Likelihood*, Springer, New-York.

Radhakrishna Rao, C. and Toutenburg, H.: 1995, *Linear Models - Least Squares and Alternatives*, Springer Series in Statistics, Springer, New-York.

Rajagopalan, B. and Lall, U.: 1998, Nearest neighbour local polynomial estimation of spatial surfaces, spatial interpolation comparison contest, *Journal of Geographic Information and Decision Analysis* **2**(2), 48–57.

Reich, R., Červenka, J. and Saouma, V.: 1997, Merlin, a three-dimensional finite element program based on a mixed-iterative solution strategy for problems in elasticity, plasticity, and linear and nonlinear fracture mechanics, *Technical report*, EPRI, Palo Alto. `http://civil.colorado.edu/~saouma/Merlin`.

Rypl, D.: 1998, *Sequential and Parallel Generation of Unstructured 3D Meshes*, PhD thesis, Czech Technical University in Prague.

Červenka, J., Chandra Kishen, J. and Saouma, V.: 1998, Mixed mode fracture of cementitious bimaterial interfaces; part II: Numerical simulation, *Engineering Fracture Mechanics*.

Verbundplan: 2001, Interpretation of measurement results; 6^{th} international benchmark workshop on numerical analysis of dams, *Technical report*, Ad Hoc Committee on COmputational Aspects of Analysis and Design of Dams, Salzburg, Austria. `www.verbundplan.at/pdf/bm_6themeC.pdf`.

Weisberg, S.: 1985, *Applied Linear Regression*, Wiley, New-York.

Wolfram, S.: 1999, *The Mathematica Book, 4^{th} Ed.*, Cambridge University Press.